LUND UNIVERSITY

Data fitting and image fine-tuning approach to solve the inverse problem in fluorescence molecular imaging

Gorpas, Dimitris; Politopoulos, Kostas; Yova, Dido; Andersson-Engels, Stefan

Published in:
IMAGING, MANIPULATION, AND ANALYSIS OF BIOMOLECULES, CELLS, AND TISSUES VI

DOI:
10.1117/12.762968

2008

Link to publication

Citation for published version (APA):
Gorpas, D., Politopoulos, K., Yova, D., & Andersson-Engels, S. (2008). Data fitting and image fine-tuning approach to solve the inverse problem in fluorescence molecular imaging. In DL. Farkas, DV. Nicolau, & RC. Leif (Eds.), *IMAGING, MANIPULATION, AND ANALYSIS OF BIOMOLECULES, CELLS, AND TISSUES VI* (Vol. 6859). SPIE. https://doi.org/10.1117/12.762968

Total number of authors:
4

General rights
Unless other specific re-use rights are stated the following general rights apply:
Copyright and moral rights for the publications made accessible in the public portal are retained by the authors and/or other copyright owners and it is a condition of accessing publications that users recognise and abide by the legal requirements associated with these rights.
• Users may download and print one copy of any publication from the public portal for the purpose of private study or research.
• You may not further distribute the material or use it for any profit-making activity or commercial gain
• You may freely distribute the URL identifying the publication in the public portal

Read more about Creative commons licenses: https://creativecommons.org/licenses/

Take down policy
If you believe that this document breaches copyright please contact us providing details, and we will remove access to the work immediately and investigate your claim.

LUND UNIVERSITY

PO Box 117
221 00 Lund
+46 46-222 00 00

Data fitting and image fine-tuning approach to solve the inverse problem in fluorescence molecular imaging

Dimitris Gorpas[1a], Kostas Politopoulos[a], Dido Yova[a], and Stefan Andersson-Engels[b]

[a] Laboratory of Biomedical Optics and Applied Biophysics, School of Electrical and Computer Engineering, National Technical University of Athens, GR-157 73, Zografou, Greece
[b] Department of Physics, Lund Institute of Technology, P.O Box 118, SE-221 00, Lund, Sweden

ABSTRACT

One of the most challenging problems in medical imaging is to "see" a tumour embedded into tissue, which is a turbid medium, by using fluorescent probes for tumour labeling. This problem, despite the efforts made during the last years, has not been fully encountered yet, due to the non-linear nature of the inverse problem and the convergence failures of many optimization techniques. This paper describes a robust solution of the inverse problem, based on data fitting and image fine-tuning techniques. As a forward solver the coupled radiative transfer equation and diffusion approximation model is proposed and compromised via a finite element method, enhanced with adaptive multi-grids for faster and more accurate convergence. A database is constructed by application of the forward model on virtual tumours with known geometry, and thus fluorophore distribution, embedded into simulated tissues. The fitting procedure produces the best matching between the real and virtual data, and thus provides the initial estimation of the fluorophore distribution. Using this information, the coupled radiative transfer equation and diffusion approximation model has the required initial values for a computational reasonable and successful convergence during the image fine-tuning application.

Keywords: Fluorescence molecular imaging, radiative transfer equation, diffusion approximation, finite elements method, fluorescence image registration, image fine-tuning.

1. INTRODUCTION

Fluorescence molecular imaging is advancing to a very essential tool for medical imaging and diagnosis[1]. The combined progress in fluorescent probes technology and imaging modalities have encountered most of the difficulties in the noise dominated fluorescence signal recording. However, data quantification and processing still lacks the feasibility and time efficacy, despite the great advantage that the computational systems technology has met during the last few years with the introduction of the multiprocessor and multi-core systems. The current state-of-the-art in fluorescence molecular imaging data processing applications require parallel programming with multiple computational units and timings in the order of many, in some cases more than ten, hours, regardless their hardware implementation, reflectance of transmittance setups. The most important reason for this lack of time efficacy is the non-linear nature of the inverse problem and the requirement of iterative procedures that would converge to a solution. However, without any prior knowledge of the fluorophore distribution, those procedures require numerous iterations to converge, if they do that at all.

The scope of the paper is to introduce a new technique for the solution of the inverse problem, which is based on data fitting and image fine-tuning and which will provide the required initial fluorophore distribution and solve the inverse problem within a few only iterations. The data fitting procedure is a very common technique among computer vision applications, especially in the field of object recognition[2, 3, 4]. Within this work the translation of this technique to the fluorescence molecular imaging was achieved. A database is constructed with image simulations of multiple tumour geometries and these images are compared to the captured one. This approach eliminates the necessity of applying the forward solver each time a new measurement is made and provides an initial guess, that is the best matching of the real fluorophore distribution. Sequentially, the image fine-tuning process utilizes the forward solver to provide the solution to the image reconstruction problem.

[1] dgorpas@mail.ntua.gr; phone +302107722293; fax +302107723894

Imaging, Manipulation, and Analysis of Biomolecules, Cells, and Tissues VI,
edited by Daniel L. Farkas, Dan V. Nicolau, Robert C. Leif,
Proc. of SPIE Vol. 6859, 68591H, (2008) · 1605-7422/08/$18 · doi: 10.1117/12.762968

Downloaded from SPIE Digital Library on 01 Jul 2011 to 130.235.188.41. Terms of Use: http://spiedl.org/terms

In order to provide a complete method for the inverse problem solution, a forward solver is also proposed which fulfills the requirements of the introduced technique. A very important prerequisite for successful data fitting application is the accuracy of the forward model. Diffusion approximation, although the golden standard of most fluorescence molecular imaging applications[5, 6], suffers from two very important, for this approach, limitations. It is not accurate close to the surface of the inspected volume and close to the excitation sources[7]. That is why it is proposed the coupled radiative transfer equation and diffusion approximation model as the forward solver[8, 9, 10]. This model utilizes the radiative transfer equation in the sub-domains of the inspected area where the assumptions of the diffusion approximation are not valid, and the diffusion approximation elsewhere. In order to compromise the time consuming radiative transfer equation solution, the finite elements method is enhanced with an adaptive multi-grid technique[11].

The outline of this paper is as follows: In Sec. 2.1 the coupled radiative transfer equation and diffusion approximation model is presented for the fluorescence molecular imaging. The forward model is consisted of a dual coupled radiative transfer equation and diffusion approximation equation system, one for the excitation field and one of the emission field, coupled through the excitation average intensity distribution. Sec. 2.2 describes the finite element approximation for the solution of the forward model. In order to accurately describe light propagation within the whole region, an adaptive multi-grid scheme can be utilized. The database models formulation is presented in Sec. 2.3. Super-ellipsoid models provide numerous simulations of fluorophore distributions. The data fitting and image fine-tuning approach is described in Sec. 2.4. All the necessary image processing algorithms are analyzed, emphasizing those that would provide the image features for the image registration between real and simulated data. The image fine-tuning process is the final step for the image reconstruction and utilizes both the forward solver and the data-fitting outcomes. Finally, in Sec. 3 some image processing results will be presented in order to strengthen this proposal by proving that the acquired fluorescence images can provide all the required features for a data fitting and image fine-tuning process with great accuracy, while some very important conclusions about this method and the following actions are discussed in Sec. 4.

2. METHODOLOGY

The image reconstruction in fluorescence imaging corresponds to the estimation of the fluorophores distribution within the object of interest, when the amount of guided light and the measured data on the boundary of the object are given. Application of computer vision techniques for the solution of the non-linear inverse problem, requires accurate description of light propagation within the medium. Thus it is essential to have a forward model that preserves high levels of accuracy at the whole region of interest.

2.1. Forward model

The coupled radiative transfer equation (RTE) and diffusion approximation (DA) model is derived by coupling RTE, with its boundary conditions, and the DA. The two models are coupled at an interface B[8, 10]. The position of this interface is determined by the scattering coefficient of the medium and it is chosen far enough from the surface, so that the DA can be considered to be a valid approximation. Furthermore, it is assumed that this interface is located within the DA sub-domain and it is actually the only boundary that the DA has. That is why, in this coupled model, the boundary condition of the DA is not applied.

In fluorescence imaging two light fields should be taken into consideration, the excitation light and the emission light. This means that a dual coupled RTE-DA model is created to compensate for both fields. For the excitation field, index exc, the only light source is the external light $I_{exc}(\mathbf{r}, \hat{\mathbf{s}})$, and thus the internal light sources are equal to zero. With the previous description for formulation of the coupled RTE-DA model, excitation light is expressed as:

$$\frac{i\cdot\omega}{c}\cdot I_{exc}(\mathbf{r},\hat{\mathbf{s}})+\hat{\mathbf{s}}\cdot\nabla I_{exc}(\mathbf{r},\hat{\mathbf{s}})+\left[\mu_{a,\,exc}(\mathbf{r})+\mu_{s,\,exc}(\mathbf{r})\right]\cdot I_{exc}(\mathbf{r},\hat{\mathbf{s}})- \mu_{s,\,exc}(\mathbf{r})\cdot\int_{4\pi} p_{exc}(\mathbf{s},\hat{\mathbf{s}}')\cdot I_{exc}(\mathbf{r},\hat{\mathbf{s}}')\cdot ds'=0 \qquad \mathbf{r}\in V_{RTE} \tag{1}$$

$$I_{exc}(\mathbf{r},\hat{\mathbf{s}})=\begin{cases}0\\ I_{src}(\mathbf{r},\hat{\mathbf{s}})\end{cases} \qquad \mathbf{r}\in S_{RTE,\,out},\ \hat{\mathbf{s}}\cdot\hat{\mathbf{n}}<0 \tag{2}$$

Downloaded from SPIE Digital Library on 01 Jul 2011 to 130.235.188.41. Terms of Use: http://spiedl.org/terms

$$I_{exc}(\mathbf{r}, \hat{\mathbf{s}}) = \frac{1}{4\cdot\pi}\cdot U_{exc}(\mathbf{r}) - \frac{3}{4\cdot\pi}\cdot\left[D_{exc}(\mathbf{r})\cdot\nabla U_{exc}(\mathbf{r})\right]\cdot\hat{\mathbf{s}} \qquad \mathbf{r}\in B \qquad (3)$$

$$\frac{i\cdot\omega}{c}\cdot U_{exc}(\mathbf{r}) - \nabla\left[D_{exc}(\mathbf{r})\cdot\nabla U_{exc}(\mathbf{r})\right] + \mu_{a,\,exc}(\mathbf{r})\cdot U_{exc}(\mathbf{r}) = 0 \qquad \mathbf{r}\in V_{DA} \qquad (4)$$

$$U_{exc}(\mathbf{r}) = \int_{4\pi} I_{exc}(\mathbf{r}, \hat{\mathbf{s}})\cdot d\hat{\mathbf{s}} \qquad \mathbf{r}\in B \qquad (5)$$

For the emission field, index em, external light source does not exist, but only the internal fluorescence sources. Thus $I_{src}(\mathbf{r}, \hat{\mathbf{s}}) = 0$ and assuming fluorophore quantum yield η, the internal light sources are described by the formalism:

$$\Lambda_{em}(\mathbf{r}) = \frac{\eta\cdot\mu_{a,\,exc}^{fluo}(\mathbf{r})}{1 - i\cdot\omega\cdot\tau(\mathbf{r})}\cdot U_{exc}(\mathbf{r}) \qquad (6)$$

where $\mu_{a,\,exc}^{fluo}(\mathbf{r})$ is the absorption coefficient of the fluorophores at the excitation wavelength and $\tau(\mathbf{r})$ is the fluorophore lifetime[12, 13, 14].

It is obvious that the fluorescence light sources are strictly depended on the solution of the coupled RTE-DA model for the excitation field. The corresponding model for the emission field is as follows:

$$\frac{i\cdot\omega}{c}\cdot I_{em}(\mathbf{r}, \hat{\mathbf{s}}) + \hat{\mathbf{s}}\cdot\nabla I_{em}(\mathbf{r}, \hat{\mathbf{s}}) + \left[\mu_{a,\,em}(\mathbf{r}) + \mu_{s,\,em}(\mathbf{r})\right]\cdot I_{em}(\mathbf{r}, \hat{\mathbf{s}}) - \mu_{s,\,em}(\mathbf{r})\cdot\int_{4\pi} p_{em}(\mathbf{s}, \hat{\mathbf{s}}')\cdot I_{em}(\mathbf{r}, \hat{\mathbf{s}}')\cdot ds' = \frac{\eta\cdot\mu_{a,\,exc}^{fluo}(\mathbf{r})}{1 - i\cdot\omega\cdot\tau(\mathbf{r})}\cdot U_{exc}(\mathbf{r}) \qquad \mathbf{r}\in V_{RTE} \qquad (7)$$

$$I_{em}(\mathbf{r}, \hat{\mathbf{s}}) = 0 \qquad \mathbf{r}\in S_{RTE,\,out},\ \hat{\mathbf{s}}\cdot\hat{\mathbf{n}} < 0 \qquad (8)$$

$$I_{em}(\mathbf{r}, \hat{\mathbf{s}}) = \frac{1}{4\cdot\pi}\cdot U_{em}(\mathbf{r}) - \frac{3}{4\cdot\pi}\cdot\left[D_{em}(\mathbf{r})\cdot\nabla U_{em}(\mathbf{r})\right]\cdot\hat{\mathbf{s}} \qquad \mathbf{r}\in B \qquad (9)$$

$$\frac{i\cdot\omega}{c}\cdot U_{em}(\mathbf{r}) - \nabla\left[D_{em}(\mathbf{r})\cdot\nabla U_{em}(\mathbf{r})\right] + \mu_{a,\,em}(\mathbf{r})\cdot U_{em}(\mathbf{r}) = \frac{\eta\cdot\mu_{a,\,exc}^{fluo}(\mathbf{r})}{1 - i\cdot\omega\cdot\tau(\mathbf{r})}\cdot U_{exc}(\mathbf{r}) \qquad \mathbf{r}\in V_{DA} \qquad (10)$$

$$U_{em}(\mathbf{r}) = \int_{4\pi} I_{em}(\mathbf{r}, \hat{\mathbf{s}})\cdot d\hat{\mathbf{s}} \qquad \mathbf{r}\in B \qquad (11)$$

Within the described model it is assumed that the presence of the fluorophores does not alter the scattering coefficient of the tissue, which means that $\mu_{s,\,exc/em}(\mathbf{r}) = \mu_{s,\,exc/em}^{tis}(\mathbf{r})$, where $\mu_{s,\,exc/em}^{tis}(\mathbf{r})$ is the scattering coefficient of the tissue. However, this is not true for the absorption coefficient, where it is assumed to be the sum between the absorption coefficient of the tissue $\mu_{a,\,exc/em}^{tis}(\mathbf{r})$ and the one of the fluorophores $\mu_{a,\,exc/em}^{fluo}(\mathbf{r})$, $\mu_{a,\,exc/em}(\mathbf{r}) = \mu_{a,\,exc/em}^{tis}(\mathbf{r}) + \mu_{a,\,exc/em}^{fluo}(\mathbf{r})$.

In the systems $(1)-(5)$ and $(7)-(11)$, $I_{exc/em}(\mathbf{r}, \hat{\mathbf{s}})$ is the specific intensity at position $\mathbf{r} = (x, y, z)^T$ for a given direction of propagation $\hat{\mathbf{s}} = (\cos\varphi\cdot\sin\theta, \sin\varphi\cdot\sin\theta, \cos\theta)^T$ where (φ, θ) are standard spherical coordinates, which flows within a unit solid angle $d\hat{\mathbf{s}}$. With ω is expressed the angular modulation frequency of the excitation source, and with c is expressed the average speed of light in the medium[7, 15]. Furthermore, $p_{exc/em}(\hat{\mathbf{s}}, \hat{\mathbf{s}}')$ is the scattering phase function, $U_{exc/em}(\mathbf{r})$ is the average intensity, and $D_{exc/em}(\mathbf{r}) = (1/3)\cdot\left[a\cdot\mu_{a,\,exc/em}(\mathbf{r}) + \mu'_{s,\,exc/em}(\mathbf{r})\right]^{-1}$ is the photon diffusion coefficient with $\mu'_{s,\,exc/em}(\mathbf{r})$ being the reduced scattering coefficient, while the factor a is related to the

Downloaded from SPIE Digital Library on 01 Jul 2011 to 130.235.188.41. Terms of Use: http://spiedl.org/terms

absorption, scattering and anisotropy of the medium. In the case of tissue this factor is in the order of $a \sim 0.5$, assuming an anisotropy factor of $g \sim 0.8$ in the visible[16]. Finally, V_{RTE} is the sub-domain of the inspected region where the RTE is applied with boundary S_{RTE} and V_{DA} is the sub-domain where the DA is valid.

The formalisms in this work are expressed in the frequency domain, however utilizing the transformation

$$i \cdot \omega \Leftrightarrow \frac{\partial}{\partial t} \tag{12}$$

one can alter the equations to time domain, or even in the steady-state condition assuming $\omega = 0$.

Under these premises, the actual scope of the fluorescence molecular imaging is to provide an accurate estimation about the positions within the inspected tissue region where the fluorophore absorption coefficient presents value different than zero, that is the actual positions of the fluorophores. Providing this information and assuming uniform distribution of the fluorophores, the three-dimensional reconstruction of the tumour embedded into tissue is feasible.

2.2. Numerical solution of the forward problem

The analytical solution of the RTE and the DA are often restricted to certain geometries, and therefore their exploitability in fluorescence molecular imaging is limited. Thus, in such applications both models are usually solved with numerical methods. The most often applied numerical methods are the finite difference method and the finite elements method[12, 17, 18]. The latter is generally regarded as more flexible when issues of implementing different boundary conditions and handling complex geometries are considered, and therefore it is most often chosen as the method for solving equations governing light transport in tissue[14, 19, 20]. The finite elements method is thus proposed as the numerical approach for the model described in the previous section.

A finite element solution of the coupled RTE-DA model can derive by posing the model in a weak variational form, instead of the strong formalisms of equations $(1)-(5)$ and $(7)-(11)$, with the use of piecewise linear functions[21, 22]. To obtain the variational formulation of this model it must be taken into consideration that the solution of the sub-system $(1)-(5)$, which is the forward model for the excitation field, is the light source element for the sub-system $(7)-(11)$, which is the forward model for the emission field. Thus, the two sub-systems will be confronted separately, with the second sub-system depending directly on the solution of the first. This will prevent the occurrence of unstable equation matrices, very important for the successful convergence to a unique solution.

Therefore, the RTE model of the two subsystems, equations (1) and (7), is multiplied with the test function $\psi(\mathbf{r}, \hat{\mathbf{s}})$ and is integrated over the sub-domain V_{RTE} and angular directions 4π, while the DA model, equations (4) and (10), is multiplied with the test function $\upsilon(\mathbf{r})$ and is integrated over the V_{DA} sub-domain. An analytical walkthrough for these integrations can be obtained from the literature[10, 21].

In order to obtain the finite element approximations of the two sub-systems, the solutions $I_{exc/em}(\mathbf{r}, \hat{\mathbf{s}})$ and $U_{exc/em}(\mathbf{r})$ of the variational formulations are approximated in piecewise linear functions per element, based on the nodal values of the above solutions. Hence, the discretizations of $I_{exc/em}(\mathbf{r}, \hat{\mathbf{s}})$ and $U_{exc/em}(\mathbf{r})$, following the Galerkin's method[21, 23, 24], are expressed as:

$$I_{exc/em}(\mathbf{r}, \hat{\mathbf{s}}) \approx I^h_{exc/em}(\mathbf{r}, \hat{\mathbf{s}}) = \sum_{i=1}^{N_n} \sum_{l=1}^{N_a} \alpha_{il,\, exc/em} \cdot \psi_i(\mathbf{r}) \cdot \psi_l(\hat{\mathbf{s}}) \tag{13}$$

$$U_{exc/em}(\mathbf{r}) \approx U^h_{exc/em}(\mathbf{r}) = \sum_{k=1}^{N} a_{k,\, exc/em} \cdot \upsilon_k(\mathbf{r}) \tag{14}$$

Downloaded from SPIE Digital Library on 01 Jul 2011 to 130.235.188.41. Terms of Use: http://spiedl.org/terms

where $\psi_i(\mathbf{r})$ and $\psi_l(\hat{\mathbf{s}})$ are the nodal basis functions of the spatial and angular finite elements discretizations of the RTE domain V_{RTE}, $\alpha_{il,\,exc/em}$ is the radiance in spatial point i and direction l, with $i = 1,\ldots,N_n$ and $l = 1,\ldots,N_a$, N_n is the number of spatial points and N_a is the number of angular directions. On the other hand, $\upsilon_k(\mathbf{r})$ are the nodal basis functions of the finite elements discretizations of the DA domain V_{DA}, $a_{k,\,exc/em}$ is the photon density in nodal point k, with $k = 1,\ldots,N$, and N is the number of nodal points.

These variable expansions are then substituted into the weak formulations of the coupled RTE-DA for the excitation or the emission field, respectively. Furthermore, as test functions are chosen the basis functions $\psi_j(\mathbf{r})$, $\psi_m(\hat{\mathbf{s}})$ and $\upsilon_p(\mathbf{r})$ alternately for all $j = 1,\ldots,N_n$, $m = 1,\ldots,N_a$ and $p = 1,\ldots,N$ in order to obtain the algebraic equations for all the unknowns. The resulting systems are linear algebraic systems, expressed in matrix mode as:

$$\begin{bmatrix} A_{RTE,\,exc/em} & B_{RTE,\,exc/em} \\ B_{DA,\,exc/em} & A_{DA,\,exc/em} \end{bmatrix} \cdot \begin{bmatrix} \alpha_{exc/em} \\ a_{exc/em} \end{bmatrix} = \begin{bmatrix} C_{RTE,\,exc/em} \\ C_{DA,\,exc/em} \end{bmatrix} \tag{15}$$

for the excitation and emission fields. In the matrix equations (15) $\alpha_{exc/em} = \left[\alpha_{il,\,exc/em}\right]$ is the radiance of excitation or emission field, respectively to the indices, in nodal points of the finite element mesh in the RTE model sub-domain, and $a_{exc/em} = \left[a_{k,\,exc/em}\right]$ is the photon density in nodal points of the finite element mesh in the sub-domain of the region where the assumptions of the DA are valid. Further, $A_{RTE,\,exc/em}$ is a block which contains the finite element approximation of the RTE as derived from the Galerkin's method, $A_{DA,\,exc/em}$ is the corresponding finite element approximation of the DA, and $B_{RTE,\,exc/em}$ and $B_{DA,\,exc/em}$ are matrices that contain the coupling connections on the interface B. The source vectors for the case of the excitation light contain in the V_{RTE} sub-domain the external light source and in the V_{DA} domain are equal to zero. On the other hand, the source vectors for the emission light contain the finite element approximation of the solution to the excitation field.

The matrix systems (15) can be solved so to provide the excitation and emission radiance in the nodal points of the spatial and angular discretizations of the RTE sub-domain and the excitation and emission photon density in the nodal points of the finite element model of the DA.

In order to avoid excessive large number of unknowns when encountered with uniform meshes, the finite element method can be enhanced with an adaptive multi-grid scheme. A coarse multi-grid T_0 is generated and over this region discretization the forward model is solved and the prediction error is estimated for each grid. The magnitude of this error determines how the multi-grids will be refined. In case the prediction error is insignificant inside a grid, then that grid will remain as it is, otherwise it will be refined and a sequence of multi-grids is constructed. However, the forward solver is not applied each time a refinement occurs, but mean nodal values are used instead and the prediction error is updated. In case the refinement is leading to significant errors, then the forward solver is applied to the new mesh. This iterative procedure is terminated only when all the multi-grids are convergent[11].

2.3. Construction of the database models

Till now the fluorescence molecular imaging applications from the forward solver proceed to the comparison between the simulated and the acquired data. This means that the time consuming forward solver must be applied each time a new measurement is made and at every iteration, till convergence occurs. The robustness of the method described in this paper is that the initial estimations of the fluorophore distribution are computed a priory, providing significant time efficacy during fluorescence molecular imaging experiments. These estimations will be stored into a database, which will be updated with every new solution. The super-ellipsoid model defines a closed surface without hole and is the most appropriate to simulate a tumour embedded into tissue. These models have been used extensively in many computer

Downloaded from SPIE Digital Library on 01 Jul 2011 to 130.235.188.41. Terms of Use: http://spiedl.org/terms

vision applications[25, 26] even in some biomedical applications[27, 28]. However, this is the first time that super-ellipsoid models are used in fluorescence molecular imaging.

A super-ellipsoid model is defined as the solution of the general form of the implicit equation:

$$f(x, y, z) = \left[\left(\frac{x}{a_1} \right)^{2/\varepsilon_2} + \left(\frac{y}{a_2} \right)^{2/\varepsilon_2} \right]^{\varepsilon_2/\varepsilon_1} + \left(\frac{z}{a_3} \right)^{2/\varepsilon_1} \tag{16}$$

In this equation, one can recognize an ellipsoid form, enriched with two more parameters, ε_1 and ε_2, that allow to control the shape curvature. More specific, ε_2 determines the shape of the super-ellipsoid cross-section parallel to the (x, y) plane, while ε_1 determines the shape of the super-ellipsoid cross-section in a plane perpendicular to the (x, y) plane and containing the z axis. As for the ellipsoid case, the a_1, a_2 and a_3 parameters are scale factors on x, y and z axis, respectively, Figure 1.

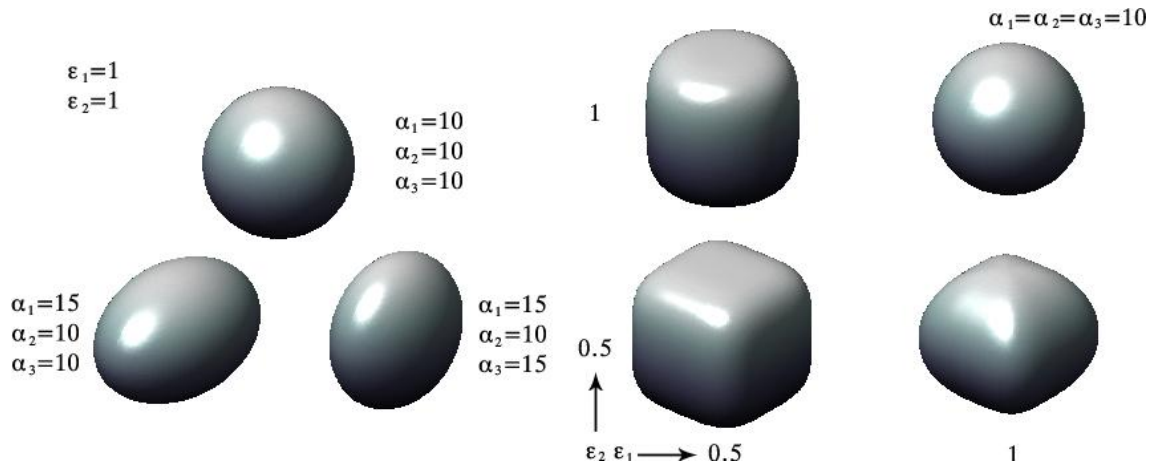

Fig. 1: Super-ellipsoid models with constant shape curvature parameters and variable scale factors (left) and constant scale factors and variable shape curvature parameters (right).

This form provides an information on the position of a three-dimensional point, related to the super-ellipsoid surface, that is important for interior/exterior determination. This information derives from the following critical values of the implicit equation, which are $f(x, y, z) = 1$ when the point lies on the surface, $f(x, y, z) < 1$ when the point is inside the super-ellipsoid, and $f(x, y, z) > 1$ when the point is outside of the super-ellipsoid. In the case of fluorophore distribution, the absorption coefficient can be expressed, utilizing these values, as:

$$\mu_{a,\, exc/em}(\mathbf{r}) = \mu^{tis}_{a,\, exc/em}(\mathbf{r}) + c \cdot \mu^{fluo}_{a,\, exc/em}(\mathbf{r}) \qquad c = \begin{cases} 1, & f(x, y, z) \le 1 \\ 0, & f(x, y, z) \le 1 \end{cases} \tag{17}$$

The expression of equation (17) is of great importance as the absorption coefficient is automatically updated for each model of the database and not user defined, as in most cases of fluorescence imaging simulations. Furthermore, the three-dimensional reconstruction of the tumour is achieved by estimation of the coefficient c in the region under inspection. Of course, there should not be ignored another six parameters, three for translation and three for rotation, that define the position of the super-ellipsoid model in a global coordinate system.

Downloaded from SPIE Digital Library on 01 Jul 2011 to 130.235.188.41. Terms of Use: http://spiedl.org/terms

Through this modeling a quite large number of simulation models are derived by only alternating the eleven parameters, required to totally describe the super-ellipsoid. These models consist the basis for populating and structuring the database, which is used for the solution of the inverse problem. The surrounding normal tissue area can be simulated by another super-ellipsoid or a rectangular area with optical properties equal to those of the tissue.

The forward solver is applied on these models and the intensity that exits the region surface is transformed to images via the expression:

$$X(\mathbf{r}) = \int_{S_{RTE,\,out}} I_{em}(\mathbf{r}, \hat{\mathbf{s}}) \cdot (\hat{\mathbf{s}} \cdot \hat{\mathbf{n}}) \cdot d\hat{\mathbf{s}} \qquad (18)$$

where $X(\mathbf{r})$ is the measurand of the system, that is the exitance on the boundary of the domain. Within this formulation losses in the imaging system are taken into consideration and accounted as a correlation factor. This factor is experimentally calculated through the system calibration process.

With the expression (18) the database is populated with simulation images, that will be used during the data fitting and image fine-tuning processes, to provide the three-dimensional reconstruction of the tumour.

2.4. Data fitting and image fine-tuning process

The acquired images for each measurement are pre-processed and normalized, in order to meet the simulation protocols of the database. The pre-processing algorithms include intensity adjustment and background correction. The background correction is achieved via subtraction of a reference background image from the primary one. The reference image will be acquired from an animal model without the presence of fluorophores so that diffuse reflectance and autofluorescence signals that pass through filters to be estimated. Further, the calibration parameters will be applied, in order to compensate for the hardware noise and distortion factors on the acquired images.

The intensity adjustment is applied to correlate intensity between captured and simulated images. Intensity adjustment is achieved via intensity mapping between high and low threshold levels. From the intensity profile of the acquired images the highest and lowest intensity values are determined and change to the threshold ones. All the other intensity levels are mapped between those borders, to avoid enhancement of some features and significant minimization of others.

Following the pre-processing procedure, a normalization of the acquired images is applied. This normalization is performed from a geometrical view point. A photogrammetric camera provides accurate three-dimensional surface reconstruction of the region under inspection. Via this procedure relative coordinates between the animal model and the imaging system are estimated and through back-projection the region under inspection can change its positioning in a global coordinates system and therefore the acquired images to be updated to that system. This global coordinates system is also used for the super-ellipsoid model development, and thus acquired and simulated images refer to the same three-dimensional coordinates. This process enhances the accuracy of the registration algorithm.

After those two image pre-processing algorithms, exactly the same features as in the database, are extracted from the acquired images. Those features include intensity profiles and geometrical information and through these features the correlation problem is confronted. Correlation maxima of intensity levels and area properties provide the correlation percentage between acquired and pre-calculated images. Threshold values of this correlation percentage provide the best matching between a super-ellipsoid model and the real tumour.

The "recovery of object shape" technique is used mainly in cases of estimation of region boundaries when the region optical properties are known a priory. Through equation (16) the super-ellipsoid model optical properties are known a priory, as well as its location inside the virtual tumour. The boundaries can then be approximated in the simulated image, and those boundaries are actually compared to the acquired images. Thus, moving backwards, information about the real prostate tumour geometry and location is derived, with a correlation factor available.

In case the overall correlation percentage exceeds a threshold value, the reconstruction problem is considered successfully solved and the three-dimensional information of the tumour is approximated by the super-ellipsoid model.

Downloaded from SPIE Digital Library on 01 Jul 2011 to 130.235.188.41. Terms of Use: http://spiedl.org/terms

This depends directly on the population size of the database, however with the super-ellipsoid models a huge number of simulations can be pre-computed, so the reconstruction problem is solved by the data fitting procedure.

On the other hand, in the case that the correlation percentage is not high enough to provide direct solution of the reconstruction problem, an image fine-tuning algorithm is applied. The inverse problem is actually the determination of the fluorophore distribution inside the region under inspection, or in other worlds the determination of the fluorophore absorption coefficient distribution. Furthermore, from equation (17) the inverse problem can be defined as the estimation of non-zero elements of the c matrix.

In order to estimate these elements, a comparison between the captured and simulated data must be accomplished. This is an optimization problem, and the quantity to be minimized (i.e. the misfit between prediction and measurement) is then:

$$F = \frac{1}{2}\left\| MS - X \right\|_S^2 \qquad (19)$$

where the norm of the difference between the actual measurements, MS , and the prediction of the emission field, X equation (18) , that exits at a part S of the surface is minimized. The actual measurements incorporate the calibration outcomes, so to compensate for any hardware distortion or noise factors and this optimization process to converge successfully. The least squares estimation technique is used to minimize equation (19) . Due to the nonlinear nature of the forward model, that provides the predicted emission field, simultaneous estimation of the parameters involves application of an iterative algorithm. For this problem, the Levenberg - Marquardt[29] optimization method has been selected as it is a virtual standard in nonlinear optimization, which significantly outperforms gradient descent and conjugate gradient methods. However, without proper initial values, the optimization may stick in a local minimum and thereby causes the convergence to fail. This problem has been confronted by using the data fitting procedure outcomes as the initial values for the optimization.

The parameters that have to be defined through this procedure are the elements of the matrix c . However, from the registration algorithm, the initial values of these parameters have been defined and they describe a rigid convex three-dimensional object inside the region under inspection. It is obvious that only surface elements of these objects will be redefined, as from the matching process it is expected that the main body of the super-ellipsoid will describe accurately the main body of the labeled tumour. This increases time efficacy, as a specific number of parameters changes after every iteration, something that does not happen when no prior information about the fluorophores distribution is available. The forward problem is solved as described previously, without further mesh refinement, as the global mesh stored into the database has been already fined enough for the real case.

When the optimization procedure converges, the real fluorophore distribution is calculated and the three-dimensional reconstruction of the embedded prostate tumour is achieved. This reconstruction model updates the database, increasing further its population. This is very important, because after a number of experimental measurements the database will provide accurate models of tumour and data fitting procedure results into correlation percentages above the threshold value. The number of experiments will be determined when the image fine tuning procedures does not occur any more. The robustness here, is that eventually the reconstruction problem is solved without the need of optimization, but only through image registration procedures.

3. RESULTS

The validity of the coupled RTE-DA model has been proven in the literature[8, 10], thus it is not included in the scope of the present work. Furthermore, the finite elements method has been also used extensively in many applications during the last few years and its results are well known and undoubted.

In this section are presented results from the main image processing algorithms that guarantee a successful data fitting and image fine-tuning process. The fluorescence image used in the following figures was acquired from a gel (1% w.v.) Agar-Agar in deionized water, on the center of which 10 μl of m-THPC solution were added. The excitation wavelength

Downloaded from SPIE Digital Library on 01 Jul 2011 to 130.235.188.41. Terms of Use: http://spiedl.org/terms

was at 405 nm and the emission maxima was at 650 nm, while proper high-pass filters were used to cut-off the reflectance and backscattering light. An acquired fluorescent image is presented in Figure 2.

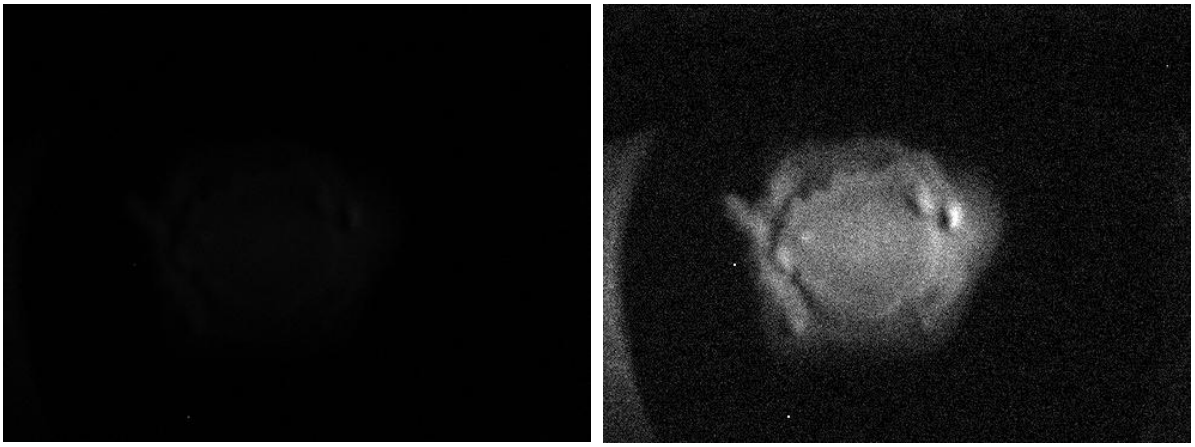

Fig. 2: Fluorescence image acquired from Agar-Agar gel (1% w.v.) with embedded m-THPC fluorophore (left) and the same image uniformly intensified for visualization reasons (right).

The intensity adjustment was performed by mapping the intensity values in each image to new values, such that values between a low threshold and a high threshold mapped to values between 0 (black) and 1 (white). Values below low and above high thresholds were clipped; that is, values below the low threshold mapped to 0 and those above the high threshold mapped to 1. For the specific protocol of image acquisition, the appropriate mapping was the one that was weighted toward higher (brighter) output values. This way, all the image elements were included in the adjusted images, even those with significant low intensity levels.

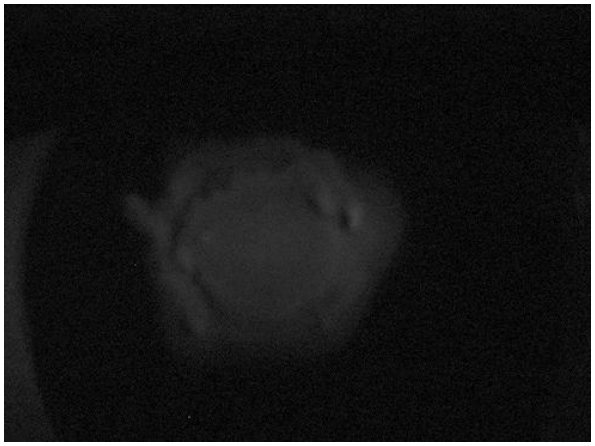

Fig. 3: Intensity adjustment in the acquired fluorescence image.

An expected side-effect of the intensity adjustment is the amplification of the inherited noise, something that is more than obvious in Figure 3. The two images were restored by implementing the Wiener filtering[30, 31]. A Wiener filter seeks an estimate $\hat{f}$ that minimizes the statistical error function expressed by the following equation:

$$e^2 = E\left\{\left(f - \hat{f}\right)^2\right\} \tag{20}$$

where E is the expressed value operator and f the undegreded image. This filter in its complete form requires the knowledge of a good deal about the signal and the properties of the noise that infects it. By considering the inherited image noise to be Gaussian the resulted restored fluorescence images are shown in Figure 4.

Downloaded from SPIE Digital Library on 01 Jul 2011 to 130.235.188.41. Terms of Use: http://spiedl.org/terms

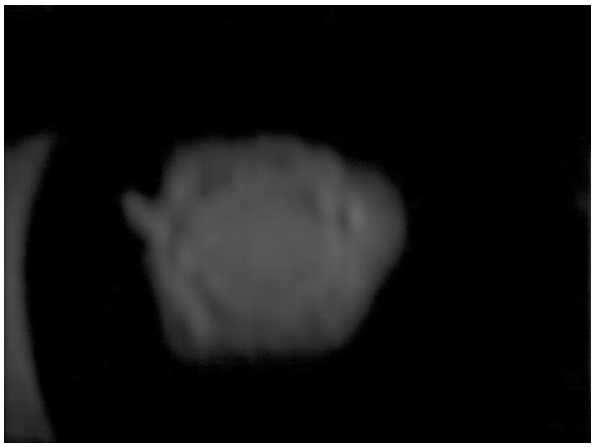

Fig. 4: Restored grey level image.

The difference between Figures 2 and 4 is sound. The images in Figure 4 were restored and they retained the details in comparison with the original images. Trying to segment the fluorescence images from the acquired ones, would result in leaving image features undetected. The reason is that the intensity of some features is quite smaller than the intensity due to inherited noise. This is most obvious close to the edges of the region.

However, the described algorithm overcame this difficulty via morphological image processing. More specific, opening filter can produce a reasonable estimate of the background across the image, as long as the selected structuring element is large enough not to fit entirely within any of the object of interest. Subtracting the resulted image from the restored, a new one with even background arises (top-hat transformation). Repeating the same procedure, but instead of opening applying the closing filter (bottom-hat transformation), and multiplying the outcomes, a contrast enhancement was succeeded, and shown in Figure 4.

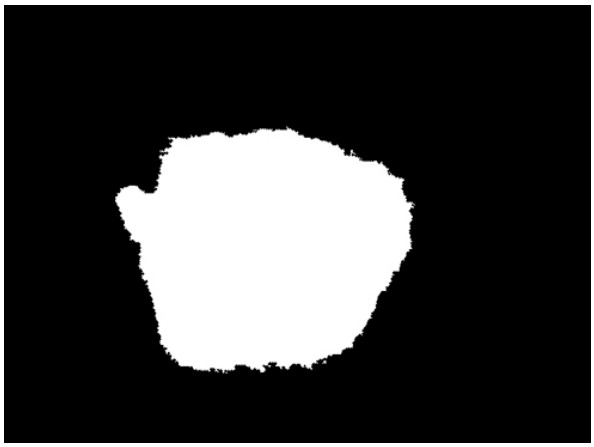

Fig. 5: Segmented image

After the preprocessing procedure the images are ready for the segmentation. Simple thresholding would lead either to the exclusion of some elements or to the region growth of others. On the other hand, application of any edge detection or segmentation algorithm would lead to falsely detected edges or over-segmentation. The reason is that the object in the images does not have sharp edges or relevant intensities. In order to avoid such problems, this algorithm performed a combination of marker-controlled watershed transformation[32, 33] and thresholding. As a result even the lowest intensity features were detected. The resulted segmented image is presented in Figure 5.

From Figure 5 all the geometrical features of the emitted fluorescence signal can be estimated. These required for the data fitting and image-fine tuning process is the area of the detected region. This feature, along with the intensity profile of the detected area can provide the correlation factor between the real and the database images.

Downloaded from SPIE Digital Library on 01 Jul 2011 to 130.235.188.41. Terms of Use: http://spiedl.org/terms

4. DISCUSSION

In this paper a new method for the solution of the inverse problem in fluorescence molecular imaging was presented. Its two main procedures, data fitting and image fine-tuning, are very promising for the translation of fluorescence molecular imaging from phantoms to animal modeling. The results from image processing showed that the fluorescence images can provide the geometrical features of the inspected region for successful data fitting.

The algorithms presented here succeeded to overcome the fact of high level noise and successfully segment the sample image. Providing this information, the image registration between database models and acquired images is feasible.

Another important aspect of the work is the proposal of the super-ellipsoids as the database models. With only eleven parameters, an excessively large number of tumour simulations can result automatically and the required initial values of the fluorophore distribution to be available. This is of great importance as the lack of these values are mostly responsible for the time consuming iterations during the solution of the inverse problem.

The method described here can be proven a valuable tool for a large number of fluorescence imaging applications. In its final formalism it is strictly related to the image acquisition system, as the calibration parameters are incorporated in the development of the database and the simulation images are constructed for a specific geometry. However, this method can be applied to any geometry, and by using any forward solver, with a cost on accuracy if the solver is not accurate enough, as long as the database is constructed in accordance to the modus operandi of the application.

5. ACKNOWLEDGMENTS

This research is supported by the EU Integrated Project “World Wide Welfare: high BRIGHTnes semiconductor lasERs for gEneric Use”, IST-2005-2.5.1 Phot.

REFERENCES

1. V. Ntziachristos, "*Fluorescence Molecular Imaging*", Annu. Rev. Biomed. Eng., **8**:1-33 (2006).
2. I. Weiss, M. Ray, “*Model-based recognition of 3D objects from single images*”, IEEE Trans. Pattern Anal. Machine Intell., **23**:116-128 (2001).
3. J.S. Ahn, B Bhanu, “*Model-based recognition of articulated objects*”, Pattern Recogn. Lett., **23**:1019-1029 (2002).
4. B. Ravichandran, A. Gandhe, R. Smith, R. Mehra, “*Robust automatic target recognition using learning classifier systems*”, Inform. Fusion, **8**:252-265 (2007).
5. E.E. Graves, J.P. Culver, J. Ripoll, R. Weissleder, and V. Ntziachristos, “*Singular-value analysis and optimization of experimental parameters in fluorescence molecular tomography*”, Opt. Soc. Am. A, **21**:231-241 (2004).
6. A. Joshi, W. Bangerth, K. Hwang, J. Rasmussen, and E. Sevick-Muraca, “*Plane-wave fluorescence tomography with adaptive finite elements*”, Optics Letters, **31**:193-195 (2006).
7. A. Ishimaru, “*Wave Propagation and Scattering in Random Media. Vol 1: Single Scattering and Transport Theory*”, Academic Press, New York (1978).
8. T. Tarvainen, M. Vauhkonen, V. Kolehmainen, and J.P. Kapio, “*Finite element model for the coupled radiative transfer equation and diffusion approximation*”, Int. J. Numer. Meth. Eng., **65**:383-405 (2005).
9. T. Vilhunen, M. Vauhkonen, V. Kolehmainen, and J.P. Kaipio, “*Linking the radiative transfer equation and the diffusion approximation*”, Biomedical Topical Meetings, The Optical Society of America, Washington, DC, USA (2002).
10. T. Tarvainen, “*Computational methods for light transport in optical tomography*”, Doctoral Dissertation, Department of Physics, University of Kuopio, Finland (2006).
11. M. Guven, B. Yazici, X. Intes, B. Chance, “*An adaptive multigrid algorithm for region of interest diffuse optical tomography*”, International Conference on Image Processing, IEEE Proc., **2**:823-826 (2003).
12. A.D. Klose and A.H. Hielscher, “*Fluorescence tomography with simulated data based on the equation of radiative transfer*”, Opt. Lett., **28**:1019-1021 (2003).
13. X. Li, “*Fluorescence and diffusive wave diffraction tomographic probes in turbid media*”, Doctoral Dissertation, University of Pennsylvania, USA (1998).
14. A. Joshi, W. Bangerth, E.M. Sevick-Muraca, “*Adaptive finite elements based tomography for fluorescence optical imaging in tissue*”, Opt. Express, **12**:5402-5417 (2004).
15. S.R. Arridge, “*Optical tomography in medical imaging*”, Inverse Probl., **15**:R41-R93 (1999).

Downloaded from SPIE Digital Library on 01 Jul 2011 to 130.235.188.41. Terms of Use: http://spiedl.org/terms

16. J. Ripoll, D. Yessayan, G. Zacharakis, V. Ntziachristos, "*Experimental determination of photon propagation in highly absorbing and scattering media*", J. Opt. Soc. Am. A, **22**:546-551 (2005).
17. A.D. Klose, V. Ntziachristos, and A.H. Hielscher, "*The inverse source problem based on the radiative transfer equation in optical molecular imaging*", J. Comput. Phys., **1**:323-345 (2005).
18. M. Francoeur, R. Vaillon, and D.R. Rousse, "*Theoretical analysis of frequency and time-domain methods for optical characterization of absorbing and scattering media*", J. Quant. Spectrosc. Radiat. Transfer, **93**:139-150 (2005).
19. J. Li, T.C. Zhu, "*Finite-element modeling of light fluence distribution in prostate during photodynamic therapy*", Proc. of COSMOL Multiphysics User's Conference, Boston, USA (2005).
20. A. Joshi, E.M. Sevick-Muraca, "*Adaptive finite elements methods for distributed parameter system identification: Applications in fluorescence enhanced frequency domain optical tomography*", Proc. of 2004 American Control Conference, Boston, USA (2004).
21. P.P. Silvester, R.L. Ferrari, "*Finite elements for electrical engineers*", Third Edition, University Press, Cambridge, United Kingdom (1996).
22. M. Guven, B. Yazici, V. Ntziachristos, "*Fluorescence optical tomography with a priory information*", Multimodal Biomedical Imaging II, Proc. SPIE, 643107 (2007).
23. D.A. French, "*Continuous Galerkin finite element methods for a forward-backward heat equation*", Numer. Meth. Part. Diff. Eqns., **15**:257-265 (1999).
24. T.K. Sengupta, S.B. Talla, S.C. Pradhana, "*Galerkin finite element methods for wave problems*", Sadhana, **30**:611-623 (2005).
25. Y. Fougerolle, A. Gribok, S. Foufou, F. Truchetet, M. Abidi, "*Implicit Surface Modeling using Supershapes and R-functions*", Proc. of Pacific Graphics '05, Macao, China (2005).
26. L. Chevalier, F. Jaillet, A. Baskurt, "*Segmentation and superquadric modeling of 3D objects*", In Proceedings of WSCG 2003, Plzen, Czech Republic (2003).
27. J.A. Tyrrell, B. Roysam, E. di Tomaso, R. Tong, E.B. Brown, R.K. Jain, "*Robust 3-D modeling of tumor microvasculature using superellipsoids*", IEEE International Symposium on Biomedical Imaging: From Nano to Macro, Arlington, Virginia, USA (2006).
28. J. Zhu, S. Zhao, Y. Ye, G. Wang, "*Computed tomography simulation with superquadrics*", Med. Phys., **32**:3136-3143 (2005).
29. JJ. More, "*The Levenberg–Marquardt algorithm: implementation and theory*", Numerical Analysis, Lect. Notes Math., **630**:105-116 (1977).
30. J.R. Parker, "*Algorithms for Image Processing and Computer Vision*",Wiley Computer Publishing, John Wiley and Sons, Inc., New York (1997).
31. A. Murli, L. D'Amore, V. De Simmone, "*The Wiener Filter and Regularization Methods for Image Restoration Problems*", In Proc. of the 10th International Conference on Image Analysis and Processing, (1999).
32. S. Beucher, "*The watershed transformation applied to image segmentation*", Scan. Microsc. Int., Suppl., **6**:299–314 (1992).
33. F. Meyer, P. Maragos, "*Multiscale morphological segmentations based on watershed, flooding, and eikonal PDE*", In: Proc. of the International Conference on Scale-Space Theories in Computer Vision (SCALESPACE' 99, Lecture Notes in Computer Science, vol. 1682), (1999).

Downloaded from SPIE Digital Library on 01 Jul 2011 to 130.235.188.41. Terms of Use: http://spiedl.org/terms